Journal of Materials Chemistry B

Accepted Manuscript

ROYAL SOCIETY OF CHEMISTRY

www.rsc.org/materialsB

Dielectric Properties of Fluorine Substituted Hydroxyapatite: Effect of the substitution on configuration of hydroxide ion chain

N. Horiuchi[1,*], J. Endo[2], N. Wada[1], K. Nozaki[1], M. Nakamura[1], A. Nagai[1], K. Katayama[2], and K. Yamashita[1]

[1]Department of Inorganic Materials, Institute of Biomaterials & Bioengineering, Tokyo Medical and Dental University, 2-3-10 Kanda-Surugadai, Chiyoda-ku, Tokyo 101-0062, Japan

[2]Department of Applied Chemistry, Tokai University, 4-1-1 Kitakaname, Hiratsuka, Kanagawa 259-1292, Japan

* Corresponding author, e-mail: nhori.bcr@tmd.ac.jp

Table of contents entry, Graphical abstracts

Dielectric properties of fluoridated hydroxyapatite (F-HAp; $Ca_5(PO_4)_3(OH)_{1-x}F_x$) were measured. The results show that the F-substitution induces the specific configuration that contains hydrogen bonds in F-HAp.

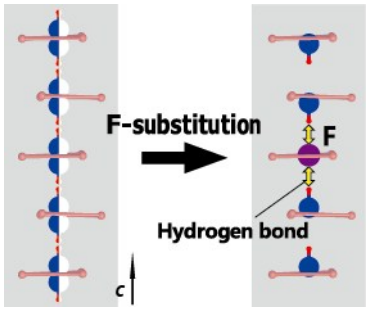

ABSTRACT

Hydroxyapatite (HAp) [$Ca_5(PO_4)_3OH$] is an extremely popular biomaterial. Moreover, HAp durability is well-known to be enhanced by fluoridation. We prepared fluoridated HAp (F-HAp; $Ca_5(PO_4)_3(OH)_{1-x}F_x$) ceramics by substituting F^- ions for OH^- ions of HAp. F-substitution dependence of dielectric properties in F-HAp was measured to detect the configuration change of OH^- ion chain. Dielectric relaxation of two kinds was observed. Each kind had a different relaxation time. Faster relaxation, which is associated with the reorientation motion of OH^- ions, was only observed at the low F-substitution range ($0 \leq x < 0.35$). The relaxation strength decreased as the F-substitution increased. It became zero at $x = 0.35$. That result suggests that F-substitution induces hydrogen bonds. One F^- ion substituted for an OH^- ion forms two hydrogen bonds with the two neighboring OH^- ions and inhibit the motion of OH^- ions, which results in some kind of ordered configuration in F-HAp. The configuration might be an origin that enhance the durability of the F-HAp.

INTRODUCTION

Hydroxyapatite (HAp), an extremely common biomaterial, is a calcium phosphate that contains hydroxyl (OH^-) ions. Those OH^- ions can be substituted for fluoride (F^-) ions, which gives F^- substituted hydroxyapatite (F-HAp; $Ca_5(PO_4)_3(OH)_{1-x}F_x$), which shows higher thermal stability[1] and mechanical strength[2], and which is practically important from the perspective of protection from dental caries.[3] That cariostatic effect derives from decreased dissolution of the teeth. F-HAp is well known to show lower solubility than HAp in an acidic atmosphere.[4] For coatings on dental implants, F-HAp is attracting interest from oral surgeons[5] because the coatings must provide long-term high stability after implantation. In fact, F-HAp coatings on a titanium substrate exhibit a lower dissolution rate than HAp.[6] Moreover, F-HAp is intriguing as a biomineral that is fabricated by living organisms. Shark teeth have particularly high fluorine content in their enamel.[7,8] Despite the importance of F-HAp for practical and academic use, few studies have examined F-HAp. Especially, quantitative research investigating the relationship between some properties and F-substitution has been lacking. As the F-substitution increases, the solubility decreased and became minimum at 50–60% of F-substitution.[4] Fracture toughness reaches its maximum value at 60% of substitution of OH by F.[2] Nevertheless, it remains unclear why F-HAp exhibits higher toughness than fluorapatite (FAp) does. The understanding of the relation between material properties and amounts of F-substitution is insufficient. Particularly, the strengthening mechanism related to F-substitution remains elusive.

In order to understand the physical and chemical properties of HAp and F-HAp, it is inevitable that we focus the role of linear chains that consist of OH^- or F^- ions in F-HAp.[9] Such

F-HAp structure has been explained in some reports of the literature.[10,11]. Some reports of the literature[10] describe that infrared spectroscopy has revealed specific configurations of the F^- and OH^- ion chains. The specific configurations (e.g., • • • OH OH F HO HO • • •, the OH orientations are changed before and after the F) are produced by bonds between F-HO. Suzuki *et al.*, using mechanical spectroscopy, observed internal friction in HAp that was attributed to the OH^- ion motion.[12] The internal friction was not observed for FAp, which does not contain OH^- ions. Results of these studies imply that a basic understanding of the strengthening of HAp by F-substitution demands investigation of OH motions. Dielectric spectroscopy can also be used to observe motions related to OH^- ions in HAp.[13–18] Those motions are expected to be influenced by the local structure and configurations. Therefore, the dielectric spectroscopy can be used to detect the structural changes in F-HAp. An earlier report[18] described the effects of F-substitution on the dielectric properties: the relaxation slowed. The activation energy was increased by F-substitution. As described herein, we prepared F-HAp sintered ceramics with different F-substitution and evaluated the dielectric properties as a function of F-substitution amounts. In addition, we discussed the configuration change of OH chain and its contribution to the strengthening mechanism of F-HAp: the relation between material properties and amounts of F-substitution is discussed.

EXPERIMENTAL

Sintered F-HAp ceramics with different F-substitution were prepared for dielectric measurements. First, stoichiometric HAp powder was synthesized from analytical grade

calcium carbonate and phosphoric acid using a wet method.[17,18] The synthesized HAp of 10.0 g and *y* mg of trifluoroacetamide (CF_3CONH_2; Wako Pure Chemical Inds. Ltd.) was mixed with 50 cm^3 of water in a ball mill with 5 mm zirconia balls (*y* = 0–1200 mg). The mixture was dried at 333 K for 24 h and was calcined at 1073 K for 2 h. The F-HAp powder obtained from calcination was mixed with 3 wt% polyvinyl alcohol water solution and was dried at 333 K for 24 h. The F-HAp powder was pressed into green compacts at 130 MPa after sieving. The green compacts were then sintered at 1523 K in water vapor or in atmosphere (*y* = 1200 mg) for 2 h. The sintered compacts had 7-mm diameter and 1-mm thickness. The surfaces were polished. Then platinum coatings were prepared as inert conductive electrodes on the surfaces using a sputtering apparatus (IB-2; Eiko Eng.). The compacts were annealed for 10 min at 873 K to improve the contact between ceramic substrates and platinum layer. Dielectric measurements were performed using an impedance analyzer (1260; Solartron Analytical). The amounts of F substitution were calculated from F^- ion contents which were determined using fluorine ion specific electrode (6561-10C; Horiba Ltd.). The calculation was based on an assumption that the all F^- ions are substituted. Densities were determined with Archimedes' method using pure water. Infrared (IR) spectra were measured using a Fourier transform infrared spectrometer (FTIR500; Jasco Corp.). Surface morphology was observed using scanning electron microscopy (S-3400NX; Hitachi Ltd.). Average grain sizes were determined using the linear intercept method. Crystal structures of F-HAp sintered compacts were evaluated using a powder X-ray diffractometer (D8 Advance; Bruker AXS) with CuKα radiation. The sample powders were mixed with a silicon powder (99.999%, Nilaco Co.) that was used as an internal standard for calculating the lattice parameters.

RESULTS

Surface morphologies for the sintered ceramics with different F-substitution are shown in Figure 1a–1i. The surfaces have no remarkable open pores, indicating that dense ceramics were prepared successfully. Average grain sizes are presented in Fig. 1j: no significant relation between the grain sizes and F-substitution was found. Figure 2 presents powder X-Ray diffraction (XRD) patterns for each sintered compact of F-HAp. The vertical axis is the square root of intensity. The green vertical lines located at the bottom of the figure are peak positions of HAp (ICDD No. 09-0432). No pattern had a peak that could be attributed to tri-calcium phosphate, calcium oxide, or any other secondary product, indicating that the sintered samples have single phase of the hexagonal apatite structure. No peak that indicates presence of monoclinic phase was found. Lattice parameters of F-HAp determined from the XRD patterns are presented in Figure 3. The lattice parameters of the *a*-axis decrease concomitantly with increased F-substitution. Those of the *c*-axis increase slightly. That behavior is the same as that described in earlier reports.[19–21] Measured densities and relative densities of F-HAp sintered compacts are portrayed in Fig. 4. The relative densities were calculated from theoretical densities calculated from the chemical formula of $Ca_5(PO_4)_3(OH)_{1-x}F_x$ and the lattice parameters in Fig. 3. The results indicate that highly dense ceramics were fabricated successfully. No considerable difference of F-substitution was found, although Gross *et al.* reported that the relative density reached its maximum value at 60% F-substitution.[21] IR adsorption spectra of F-HAp are presented in Fig. 5. Absorbance bands at 670, 715, 735, and 3540 cm^{-1}, which are indicated by vertical red lines in the figure, are those involving F-substitution.[10,11,19] The band intensities changed with F-substitution. These behaviors are

entirely consistent with a report of an earlier study[10]. The results demonstrate that the OH^- ions were substituted to F^- ions. The absorbance at 3570 cm^{-1} is attributed to OH^- stretching. When some OH^- ions are substituted to F^- ions, some OH-F hydrogen bonds are formed. The hydrogen bonds cause the bands at 3540 cm^{-1}. This band was observed at x = 0.89, suggesting that the OH^- ions still remain in the F-HAp.

Figure 1. (a)–(i) Surface morphologies of F-HAp for different F-substitution. (j) Grain sizes as a function of F-substitution x in the formula of $Ca_5(PO_4)_3(OH)_{1-x}F_x$.

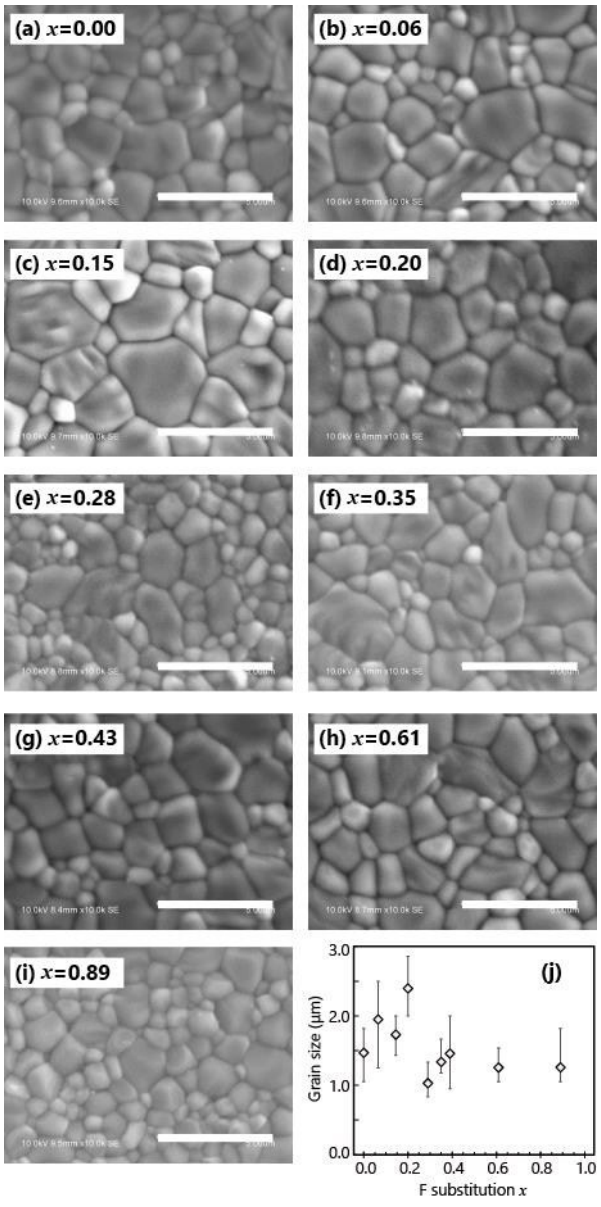

Figure 2. XRD patterns for F-HAp with different F-substitution. The vertical axis shows the square root of the intensity. Peaks denoted by the triangle marks are derived from silicon powder.

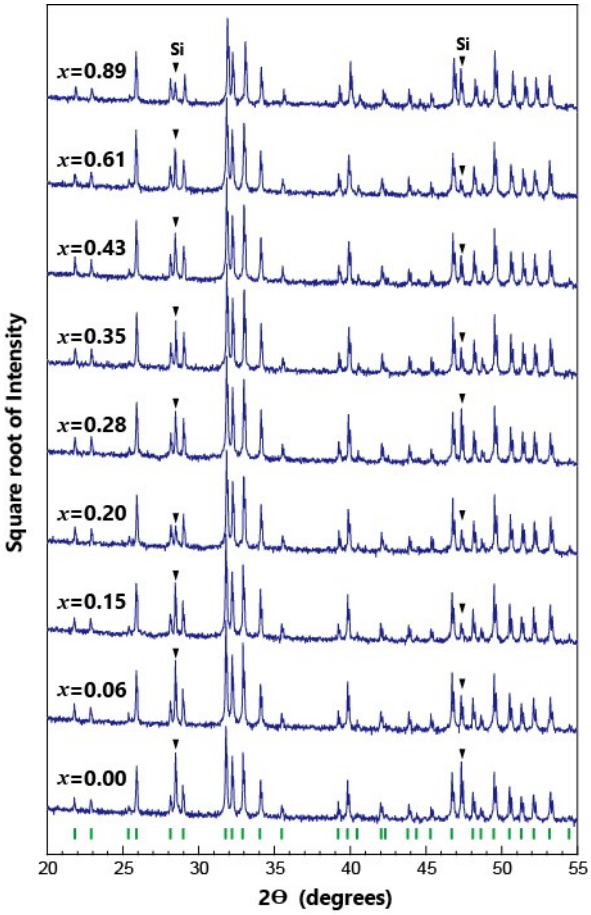

Figure 3. Lattice parameters of F-HAp determined from the XRD patterns.

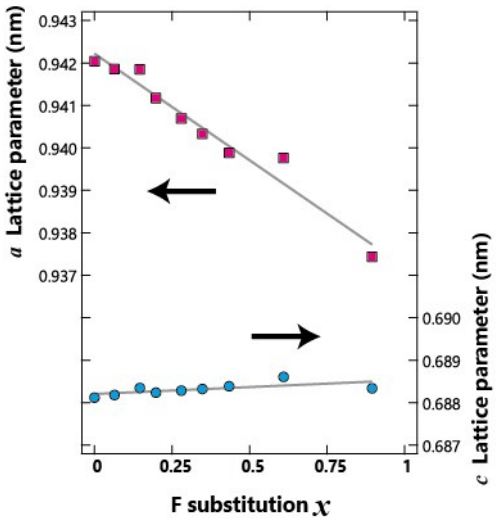

Figure 4. Measured densities and relative densities of F-HAp.

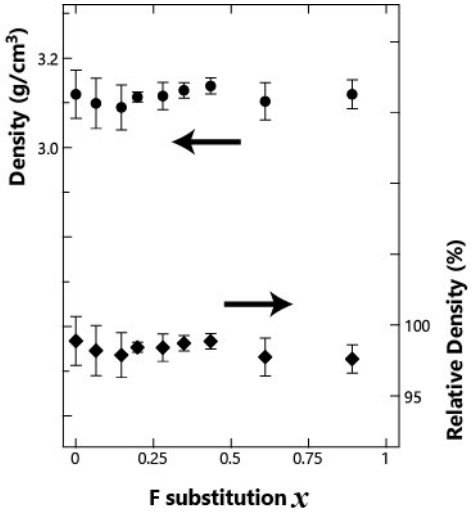

Figure 5. Infrared spectra of F-HAp. Peaks related to F-substitution are shown as the red vertical lines.

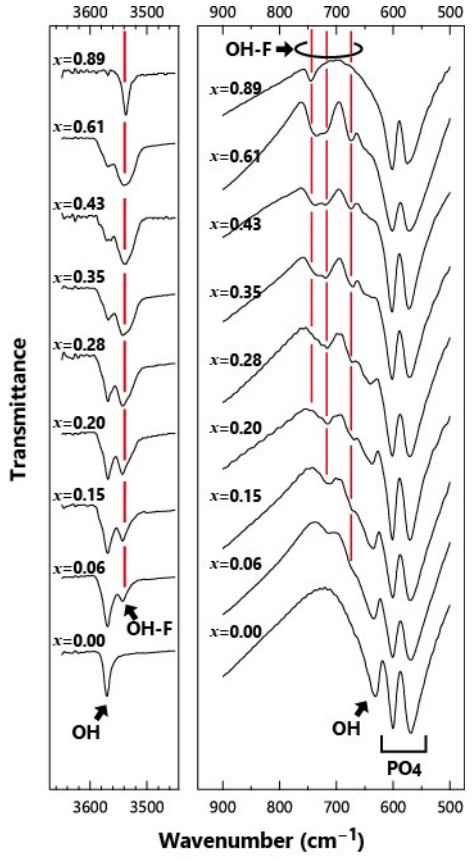

Figure 6 shows the relative permittivity as a function of frequency for F-HAp with (a)(b) x = 0.06 and (c)(d) x = 0.35. The marks are experimental data. Solid lines are calculated data. As shown in Figure 6a and 6b, the F-HAp with x = 0.06 has two-step dielectric relaxation. In

the real part of permittivity portrayed in Figure 6a, a two-step decrease was observed. The two peaks are observed in Figure 6b. Two-step relaxation was observed also in other studies.[15,17,18] One is located at the lower frequency range, with large relaxation strength (60–500). The other is at higher frequency range, and has smaller relaxation strength (20–60). These relaxations located at lower and higher frequency ranges are designated respectively as relax_L (low) and relax_H (high) for simplicity. In contrast, Figures 6c and 6d show only one relaxation. The permittivity of F-HAp with $x = 0.35$ has no relax_H.

Figure 6. Relative permittivity as a function of frequency for F-HAp with x = 0.06 and 0.35. (a) Real part and (b) imaginary part for F-HAp (x = 0.06) and (c) real and (d) imaginary part for F-HAp (x = 0.35). Marks are measured values. Solid lines show calculated results.

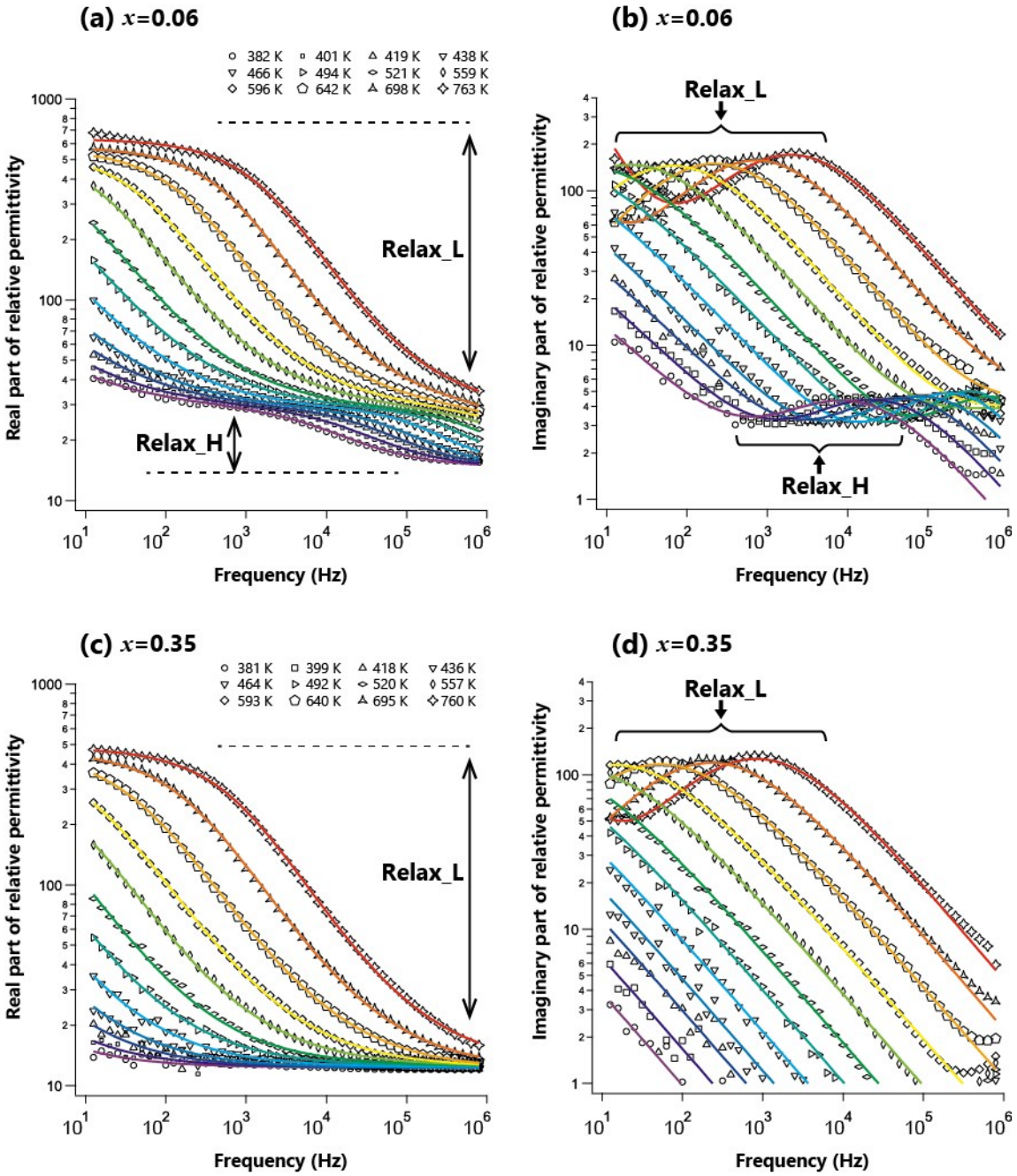

We attempted to evaluate the relaxation processes using the equation

$$\varepsilon^*(\omega) = i\frac{\sigma_{DC}}{\omega} + \frac{\varepsilon_{\mathrm{L}}}{1+(i\omega\tau_{\mathrm{L}})^{\beta_{\mathrm{L}}}} + \frac{\varepsilon_{\mathrm{H}}}{1+(i\omega\tau_{\mathrm{H}})^{\beta_{\mathrm{S}}}} + \varepsilon_0, \qquad (1)$$

which is based on the Cole–Cole equation.[22] Therein, $\varepsilon^*(\omega)$ is the complex relative permittivity as a function of angular frequency ω, ε_0 is the relative permittivity in the high-frequency limit,

ε_L and ε_H respectively denote the relaxation strength of relax_L and relax_H, and τ_L and τ_H respectively represent the relaxation times of relax_L and relax_H. Also, β_L and β_S ($0 < \beta_i \leq 1$) are the parameters used to describe different relaxation shapes. The relaxation peaks become broader as β decreases from $\beta = 1$. When $\beta = 1$, the Cole–Cole equation reduces to the Debye model. σ_{DC} is the parameter for depicting the DC conductivity. The experimental data of the real and imaginary relative permittivity were fitted with equation 1 using a least-squares program. Good fit was obtained as shown in Figure 6; the solid lines show calculated data. The obtained parameters are presented in Figures 7 and 8. The values of τ_H and τ_L are presented as a function of inverse temperature in Figure 7. The values of ε_L, ε_H, and ε_0 are shown in respectively in Figure 8a–8c, and the values varied with the temperature but showed no significant dependence on temperature, therefore, the variations are shown by error bars in the figure. The obtained parameters β_L and β_S are 0.53–0.83, however, which have no significant difference among different F-substitutions. As shown in Figure 8a, the values of ε_L were about 100–600, which decrease concomitantly with increasing F-substitution. The values of ε_H also decreased concomitantly with increasing F-substitution. It is noteworthy that ε_H decrease steeply, becoming zero at $x = 0.35$. Furthermore, relax_H was not observed at higher F-substitution. The values of ε_0 (shown in Figure 8c) also decreased concomitantly with increasing F-substitution, from 21 at $x = 0.00$ to 8 at $x = 0.89$. These ε_0 values are comparable with values reported from earlier studies.[17,24,25] The decrease of ε_0 implies that the lattice vibration also changes with F-substitution. In Figure 7, the marks at the high temperature range denote relaxation times for relax_L (τ_L). The marks at the low temperature range denote those for relax_H (τ_H). The τ_H for $x = 0.35$, 0.43, and 0.61 were not represented because relax_H was

not observed in these compositions. It is noteworthy that τ_L for F-HAp are one order of magnitude larger than that of HAp (x = 0.00). All series can be fitted well by the straight lines, indicating that these relaxation times can be described by the Arrhenius equation: $\tau = \tau_0 \exp(-E_i/kT)$, where k is Boltzmann's constant, and where E_i is the activation energy for relax_L and relax_H (E_L and E_H, respectively). The E_L and E_H values were calculated from the slope of the lines in Figure 7, which are presented in Figure 8d. The activation energy for relax_L (E_L) increased concomitantly with increasing F-substitution. It reached its maximum value at x = 0.35. The behavior of ε_H and E_L as a function of the F-substitution (Figures 8b and 8d) implies that the F-substitution of x = 0.33 is an important value in relation to F-HAp.

Figure 7. Relaxation times of relax_L and relax_H for F-HAp with different F-substitution.

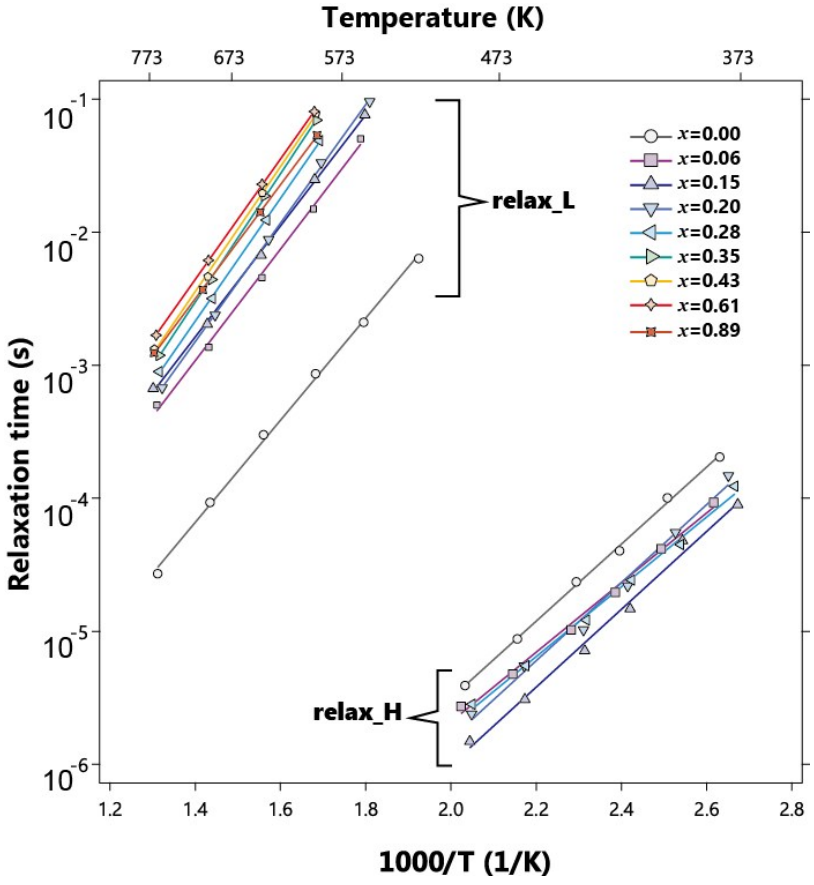

Figure 8. F-substitution x dependence of (a) ε_L, (b) ε_H, (c) ε_0, and (d) activation energy for relax_L and relax_H.

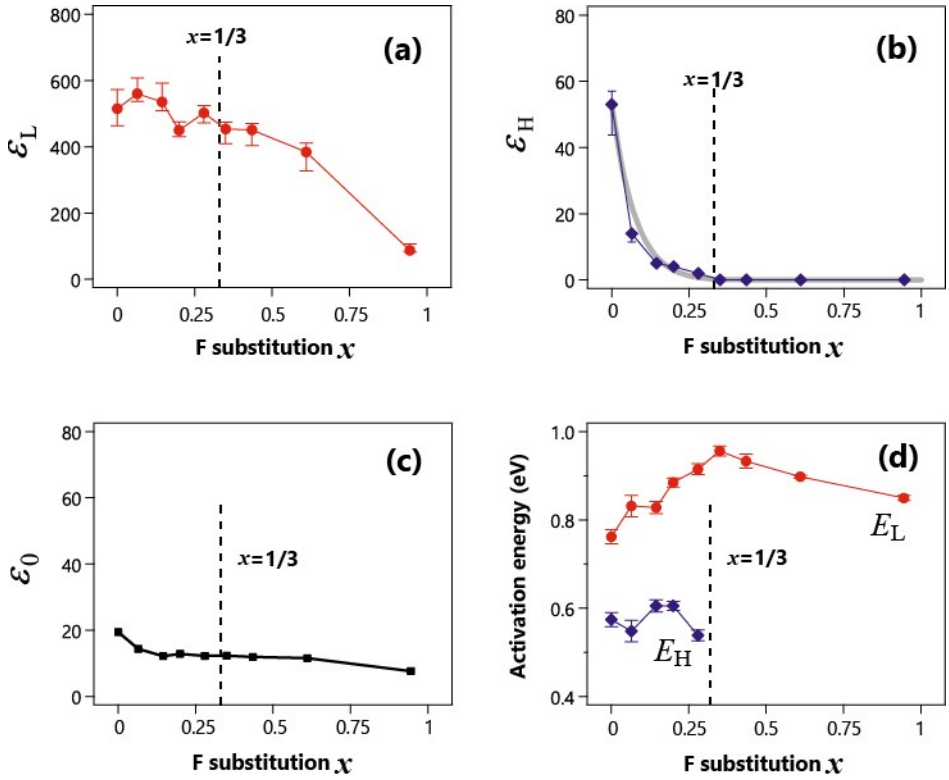

DISCUSSION

Figure 9a–9d portray crystal structures for HAp, FAp, or F-HAp. Figure 9a is a crystal structure of HAp that is a projection onto the *ab*-plane. The calcium triangles (circled with broken line) form tunnels along the *c*-axis. In the tunnels, OH^- ions are aligned as shown in Figure 9b.[11] The half-filled color of OH^- ions denotes that the occupancy of OH^- ions upward and downward of Ca-triangle is 0.5 in hexagonal HAp. Where all the OH^- ions are substituted into F^- ions, FAp is provided as shown in Figure 9c, the tunnel for FAp.[11] Figure 9d shows the tunnel for F-HAp, where an OH^- ion was replaced by the F^- ions. The F^- ion generates hydrogen bonds between the protons of neighboring OH^- ions, as suggested by IR measurements in Fig. 5.[10,11] Structural analysis also suggested the substituted F^- ions create hydrogen bonds.[20]

Figure 9. (a) Crystal structure of HAp projected onto the *ab*-plane. (b)(c) Schematic illustration of the OH^- and F^- ions aligning the along *c*-axis.

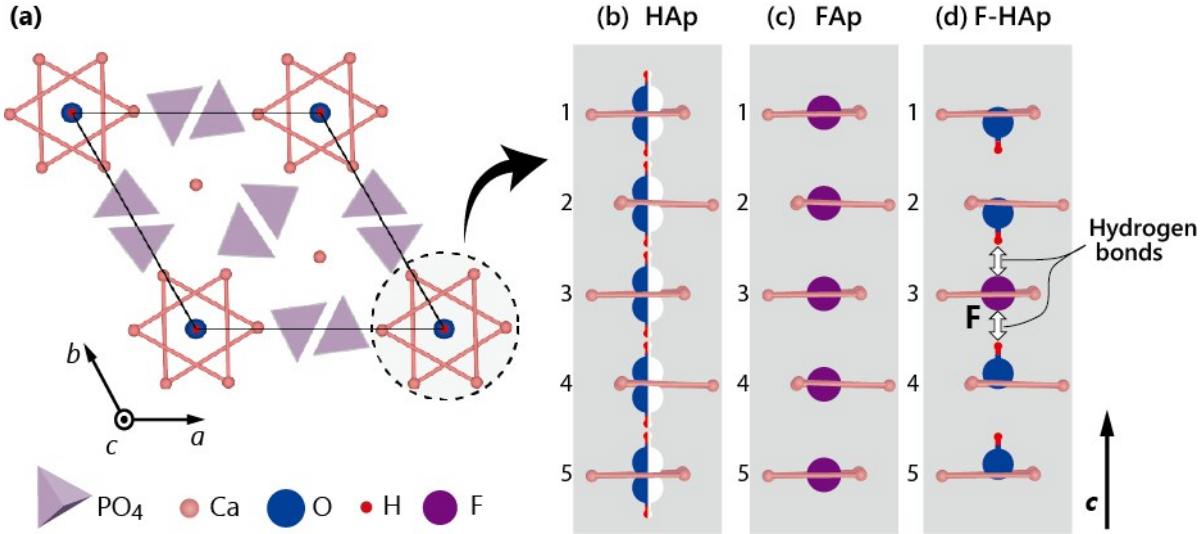

The observed dielectric relaxations (relax_H and relax_L) originate from the motions of OH^- ions in the Ca-tunnels in the HAp crystal. The relax_H can be attributed to reorientation of the electrical dipoles of OH^- ions. Arends *et al.* and Ikoma *et al.* also reported the two dielectric relaxations and discussed that the one relaxation was attributed to the reorientation of hydroxyl ions.[13,15] Our previous report[17] compared dielectric behaviors of dehydrated and normal HAp and presented that relax_H resulted from reorientation of the electrical dipoles of OH^- ions. Dehydration induces defects of OH^- ions and proton vacancies as the following reaction: $Ca_{10}(PO_4)_6(OH)_2 \rightarrow Ca_{10}(PO_4)_6(OH)_{2-2x}O_x\square_x + xH_2O(g)$, where □ denotes vacancies. The reaction decreases the OH^- ions and results in decreasing of the relaxation strength of relax_H (ε_H). As for the relax_L, it can be attributed to proton conduction.[17] In HAp, proton conductions were observed.[24–27] The protons migrate along the *c*-axis using the proton defects (defects of OH^- ions). The protons in HAp decrease with the F-substitution increasing. The decrease of proton might induce a decrease of the proton conduction. Indeed, in Figure 8a, the relaxation strength is shown to decrease as the F-substitution increased.

The OH^- ion reorientation of relax_H is the flapping motion shown in Figure 10. The OH^- ion located downward of the Ca-triangle turns upward and vice versa. The detailed path of the reorientation motion was visualized using a combination technique incorporating X-ray diffraction, neutron diffraction, and bond valence method.[27,28] This kind of OH^- reorientation has been discussed in many reports of the literature because the orientation of OH^- ions is involved with the phase transition[29–31] between monoclinic phase (OH^- ordered phase) and hexagonal phase (OH^- disordered phase). Hitmi *et al.* studied co-operative motion of OH^- reorientation using the thermally stimulated current technique.[32,33] The reorientation has compensation temperature of 484 K, which is near the phase transition temperature. The OH^- motion was studied using molecular dynamics (MD) simulations.[31] The simulation suggested that the reorientations were observed at the temperature of approximately 473 K.

Figure 10. Schematic illustrations of OH^- ion reorientation.

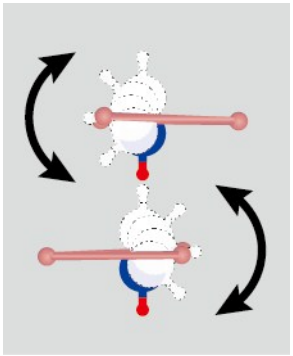

The dielectric behaviors of F-HAp, the F-substitution dependence of the dielectric relaxations (relax_L and relax_H), are well understood by presuming that the configuration shown in Figure 9d is induced to F-HAp. The substituted F^- ion forms two hydrogen bonds

between the neighbor OH^- ions. Figure 8b shows that the ε_H steeply decreased and became zero at $x \geq 0.35$ because the hydrogen bond that caused by F-substitution immobilizes the OH^- reorientation. As the F-substitution increases, the mobile (in other word, *uncaptured* by the hydrogen bonds) OH^- ions decrease as the F-substitution increases. The lines presented in Figure 11a were the ratio of uncaptured OH^- ions, which were calculated on the assumption that the F^- and OH^- ions were arrayed randomly along the *c*-axis. As shown in the figure, the mobile (uncaptured) OH^- ions decrease steeply as the F-substitution increases. Numbers with lines (1–6) in the figure indicate the index of OH^- ions that are immobilized by one F-substitution. For example, the case of number 3 is presented in the inset of Figure 11a. The OH^- ions up to the third nearest neighbor are immobilized by one F-substitution. As the index number increases, the rate of decrease increases; the uncaptured OH^- ions decreases more and more steeply. The line of number 6 is presented in Figure 8b as a thick line. Good agreement can be found between the calculated line and the experimentally obtained result, suggesting that one F^- ion substitution stops the motions of up to 6^{th} neighbor OH^- ions in the dilute F-substitution area. The activation energy of relax_L (E_L) became maximum at $x = 0.35$, as shown in Figure 8d. This is explainable by the number of induced hydrogen bonds that are induced by F-substitution. Figure 11b presents the number of hydrogen bonds as a function of F-substitution, as obtained from the calculation which assumed that randomly arranged chains of OH^- and F^- ions. The induced hydrogen bonds are most numerous at around $x = 0.38$ because the additional F-substitution does not increase the hydrogen bonds, but it increases F-F chains (a configuration formed when one F^- ion is located next to another F^- ion). The hydrogen bond number can be expected to affect the activation energy of relax_L (E_L). Proton conduction is

inhibited by the hydrogen bonds. Therefore the (E_L) has a peak at x = 0.35.

Figure 11. Calculation results of (a) number of uncaptured OH^- ions and (b) number of hydrogen bonds in F-HAp.

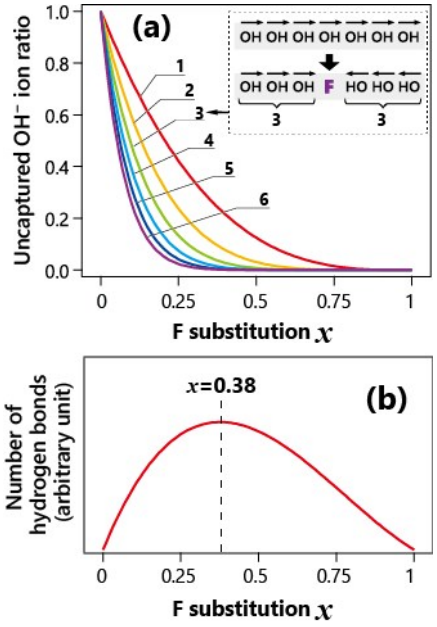

As discussed above, the dielectric properties depend on the F-substitution. The results imply that the configuration that was formed by F-substitution for OH^- ions: one F^- ion formed two hydrogen bonds with the neighboring two OH^- ions, as shown in Figure 9d. The configuration might contribute to the increase F-HAp stability and durability. A dissolution mechanism of F-HAp was suggested[34,35]: The first step of dissolution is an exchange reaction of one OH^- ion with water molecule, and the exchange results in a local instability. The first step can be hindered by the configuration including the hydrogen bonds, which may prevent the dissolution of F-HAp. In F-HAp, the chemical stability and mechanical strength increase as the F-substitution increase. However, they reach maximum values not at a high F-substitution level but at the middle F-substitution area (50–60% of F-substitution).[2,4] The reason can be explained using the configuration that is induced by the F-substitution. As shown in Fig. 11, the

number of hydrogen bond become maximum at the middle F-substitution area. The maximum number of hydrogen bonds provide maximum durability at the middle F-substitution area.

CONCLUSIONS

We studied the F-substitution dependence of dielectric properties in F-HAp, $Ca_5(PO_4)_3(OH)_{1-x}F_x$. Two kinds of dielectric relaxation were observed. One relaxation was observed at higher frequency (relax_H), which was ascribed to the reorientation motion of OH^- ions. Another relaxation observed at lower frequency (relax_L) was attributed to proton conduction. Relax_H was observed only at $x < 0.35$. The relaxation strength decreases steeply with increasing F-substitution. Regarding relax_L, the activation energy became maximum at $x = 0.35$. These behaviors of dielectric properties imply that the specific configuration that contains hydrogen bonds was induced by the F-substitution. A F^- ion substituted for one OH^- forms two hydrogen bonds with the neighboring OH^- ions. The configuration might contribute to the increase F-HAp stability and durability.

ACKNOWLEDGMENTS

This work was partially supported by JSPS KAKENHI Grant Number 23300178. One of the authors (N.H.) appreciates a grant from the Kazuchika Okura Memorial Foundation (2012).

REFERENCES

1 Y. Chen and X. Miao, *Biomaterials*, 2005, **26**, 1205–1210.
2 K. A. Gross and L. M. Rodríguez-Lorenzo, *Biomaterials*, 2004, **25**, 1385–1394.
3 R. Shellis and R. Duckworth, *Int. Dent. J.*, 1994, **44**, 263–273.
4 E. C. Moreno, M. Kresak and R. T. Zahradnik, *Nature*, 1974, **247**, 64–65.

5 I. Heling, R. Heindel and B. Merin, *J. Oral Implantol.*, 1981, **9**, 548–555.
6 H.-W. Kim, H.-E. Kim and J. C. Knowles, *Biomaterials*, 2004, **25**, 3351–3358.
7 J. Enax, O. Prymak, D. Raabe and M. Epple, *J. Struct. Biol.*, 2012, **178**, 290–299.
8 C. Chen, Z. Wang, M. Saito, T. Tohei, Y. Takano and Y. Ikuhara, *Angew. Chem. Int. Ed.*, 2014, **53**, 1543–1547.
9 V. Uskoković, *RSC Adv.*, 2015, **5**, 36614–36633.
10 F. Freund and R. M. Knobel, *J. Chem. Soc. Dalton Trans.*, 1977, 1136–1140.
11 J. C. Elliott, *Structure and chemistry of the apatites and other calcium orthophosphates*, Elsevier, 1994.
12 S. Suzuki, M. Sakamura, M. Ichiyanagi and M. Ozawa, *Ceram. Int.*, 2004, **30**, 625–627.
13 J. Arends, B. S. H. Royce, J. Siegel and R. Smoluchowski, *Phys. Lett. A*, 1968, **27**, 720–721.
14 V. P. Orlovskii, N. A. Zakharov and A. A. Ivanov, *Inorg. Mater.*, 1996, **32**, 654–656.
15 T. Ikoma, A. Yamazaki, S. Nakamura and M. Akao, *J. Mater. Sci. Lett.*, 1999, **18**, 1225–1228.
16 S. A. M. Tofail, D. Haverty, K. T. Stanton and J. B. McMonagle, *Ferroelectrics*, 2005, **319**, 117–123.
17 N. Horiuchi, J. Endo, N. Wada, K. Nozaki, M. Nakamura, A. Nagai, K. Katayama and K. Yamashita, *J. Appl. Phys.*, 2013, **113**, 134905.
18 N. Horiuchi, J. Endo, K. Nozaki, M. Nakamura, A. Nagai, K. Katayama and K. Yamashita, *J. Ceram. Soc. Jpn.*, 2013, **121**, 770–774.
19 A. Baumer, M. Ganteaume and W. Klee, *Bull. Mineral.*, 1985, **108**, 145–152.
20 L. M. Rodríguez-Lorenzo, J. N. Hart and K. A. Gross, *J. Phys. Chem. B*, 2003, **107**, 8316–8320.
21 K. A. Gross and L. M. Rodríguez-Lorenzo, *Biomaterials*, 2004, **25**, 1375–1384.
22 K. S. Cole and R. H. Cole, *J. Chem. Phys.*, 1941, **9**, 341–351.
23 J. P. Gittings, C. R. Bowen, A. C. E. Dent, I. G. Turner, F. R. Baxter and J. B. Chaudhuri, *Acta Biomater.*, 2009, **5**, 743–754.
24 T. Takahashi, S. Tanase and O. Yamamoto, *Electrochimica Acta*, 1978, **23**, 369–373.
25 K. Yamashita, H. Owada, T. Umegaki, T. Kanazawa and K. Katayama, *Solid State Ion.*, 1990, **40–41, Part 2**, 918–921.
26 K. Yamashita, K. Kitagaki and T. Umegaki, *J. Am. Ceram. Soc.*, 1995, **78**, 1191–1197.
27 M. Yashima, N. Kubo, K. Omoto, H. Fujimori, K. Fujii and K. Ohoyama, *J. Phys. Chem. C*, 2014, **118**, 5180–5187.
28 M. Yashima, Y. Yonehara and H. Fujimori, *J. Phys. Chem. C*, 2011, **115**, 25077–25087.
29 J. C. Elliott, P. E. Mackie and R. A. Young, *Science*, 1973, **180**, 1055–1057.
30 H. B. Van Rees, M. Mengeot and E. Kostiner, *Mater. Res. Bull.*, 1973, **8**, 1307–1309.
31 O. Hochrein, R. Kniep and D. Zahn, *Chem. Mater.*, 2005, **17**, 1978–1981.
32 N. Hitmi, C. LaCabanne and R. A. Young, *J. Phys. Chem. Solids*, 1986, **47**, 533–546.
33 N. Hitmi, C. LaCabanne and R. A. Young, *J. Phys. Chem. Solids*, 1988, **49**, 541–550.
34 S. V. Dorozhkin, *J. Cryst. Growth*, 1997, **182**, 133–140.
35 S. V. Dorozhkin, *J. Colloid Interface Sci.*, 1997, **191**, 489–497.

Dielectric properties of fluoridated hydroxyapatite (F-HAp; $Ca_5(PO_4)_3(OH)_{1-x}F_x$) were measured. The results show that the F-substitution induces the specific configuration that contains hydrogen bonds in F-HAp.